^{64}Cu antibody-targeting of the T-cell receptor and subsequent internalization enables in vivo tracking of lymphocytes by PET

Christoph M. Griessinger[a], Andreas Maurer[a], Christian Kesenheimer[a], Rainer Kehlbach[b], Gerald Reischl[a], Walter Ehrlichmann[a], Daniel Bukala[a], Maren Harant[a], Funda Cay[a], Jürgen Brück[c], Renate Nordin[c], Ursula Kohlhofer[d], Hans-Georg Rammensee[e,f], Leticia Quintanilla-Martinez[d], Martin Schaller[c], Martin Röcken[c], Bernd J. Pichler[a,1], and Manfred Kneilling[a,c]

[a]Department of Preclinical Imaging and Radiopharmacy, Werner Siemens Imaging Center, [b]Department of Diagnostic and Interventional Radiology, [c]Department of Dermatology, [d]Department for Pathology, and [e]Department of Immunology, Eberhard Karls University, 72076 Tübingen, Germany; and [f]German Cancer Consortium, German Cancer Research Center Partner Site Tübingen, 72076 Tübingen, Germany

Edited by Owen N. Witte, Howard Hughes Medical Institute, University of California, Los Angeles, CA, and approved December 22, 2014 (received for review September 24, 2014)

T cells are key players in inflammation, autoimmune diseases, and immunotherapy. Thus, holistic and noninvasive in vivo characterizations of the temporal distribution and homing dynamics of lymphocytes in mammals are of special interest. Herein, we show that PET-based T-cell labeling facilitates quantitative, highly sensitive, and holistic monitoring of T-cell homing patterns in vivo. We developed a new T-cell receptor (TCR)-specific labeling approach for the intracellular labeling of mouse T cells. We found that continuous TCR plasma membrane turnover and the endocytosis of the specific ^{64}Cu-monoclonal antibody (mAb)–TCR complex enables a stable labeling of T cells. The TCR–mAb complex was internalized within 24 h, whereas antigen recognition was not impaired. Harmful effects of the label on the viability, DNA-damage and apoptosis-necrosis induction, could be minimized while yielding a high contrast in in vivo PET images. We were able to follow and quantify the specific homing of systemically applied ^{64}Cu-labeled chicken ovalbumin (cOVA)-TCR transgenic T cells into the pulmonary and perithymic lymph nodes (LNs) of mice with cOVA-induced airway delayed-type hypersensitivity reaction (DTHR) but not into pulmonary and perithymic LNs of naïve control mice or mice diseased from turkey or pheasant OVA-induced DTHR. Our protocol provides consequent advancements in the detection of small accumulations of immune cells in single LNs and specific homing to the sites of inflammation by PET using the internalization of TCR-specific mAbs as a specific label of T cells. Thus, our labeling approach is applicable to other cells with constant membrane receptor turnover.

PET imaging | mouse T cells | in vivo cell tracking | antibody-based cell labeling | airway DTHR

Noninvasive in vivo imaging is an emerging method that enables the examination of T-cell migration kinetics, homing patterns, and the sites of T-cell proliferation and activation. These data are needed for a better understanding of the T-cell response during autoimmune diseases, allergies, infections, and cancer (1). Furthermore, this method reveals the basic mechanisms required for the understanding of T-cell-based immunotherapies and the development and optimization of personalized therapies (2). $CD4^+$ IFN-γ–producing T-helper cells (TH1) and IL-4–producing T-helper cells (TH2) are key players in organ-specific autoimmune diseases, such as multiple sclerosis, rheumatoid arthritis, bronchial asthma, and insulin-dependent diabetes mellitus (3). In addition, tumor-associated antigen-specific TH1 cells can inhibit tumor growth (2, 4–6). However, the exact mode of action, as well as the sites of in vivo homing, proliferation, and trafficking kinetics remain unknown for most immune cells; therefore, noninvasive imaging tools are required to visualize their location and trafficking patterns to enable organ-specific temporal quantification.

For in vivo investigation of physiological lymphocyte trafficking, it is strictly required to establish a labeling method with little or no impairment to lymphocyte viability and functionality. One frequently used cell-labeling compound for PET is [^{64}Cu]Pyruvaldehyde bis(N^4-methylthiosemicarbazone) ([^{64}Cu]PTSM), which has been applied to mouse lymphocytes, primate stem cells, and human dendritic cells (7–9). We recently established a [^{64}Cu]PTSM-labeling protocol that minimizes the harmful effects on T-cell functions (10). Nevertheless, intracellular [^{64}Cu]PTSM labeling continues to impair viability and functionality as well as to induce apoptosis/necrosis and DNA damage in TH1 cells. The use of T-cell receptor (TCR)-specific radiolabeled monoclonal antibodies (mAbs) as a label might minimize the harmful effects of ^{64}Cu on lymphocytes compared with [^{64}Cu]PTSM labeling.

Our study aimed to develop a new, highly specific intracellular labeling strategy for T cells that enables whole-body, noninvasive in vivo T-cell tracking. We targeted the antigen-specific TCR using radiolabeled mAbs. We labeled chicken-ovalbumin-TCR-transgenic TH1 cells (cOVA-TCRtg-TH1) with ^{64}Cu-DOTA–modified cOVA-TCR–specific mAbs in vitro and investigated the endocytosis-dependent intracellular accumulation of the mAb–TCR complex. We performed temporal and quantitative PET imaging of systemically transferred and labeled

Significance

Noninvasive tracking of T cells is an important method to reveal basic mechanisms of T-cell–based immunotherapies. Herein, to our knowledge we show for the first time that intracellular labeling of mouse lymphocytes for in vivo PET can be achieved by targeting membranous T-cell receptors with specific ^{64}Cu-coupled antibodies because of a continuous plasma membrane turnover. This direct-labeling method provides impressive advantages compared with common radioactive labeling methods, like [^{64}Cu]PTSM or [^{111}In]oxin, with regard to minimized influences on the target cells, while providing a high labeling stability and contrast. Thus, in noninvasive in vivo cell-tracking PET studies, we could follow the specific homing of T cells into inflamed tissues. Consequently, this method is easily transferable to other immune cell populations.

Author contributions: C.M.G., H.-G.R., M.R., B.J.P., and M.K. designed research; C.M.G., A.M., D.B., M.H., F.C., J.B., R.N., and U.K. performed research; A.M., C.K., G.R., W.E., and M.S. contributed new reagents/analytic tools; C.M.G., R.K., and L.Q.-M. analyzed data; and C.M.G., M.R., B.J.P., and M.K. wrote the paper.

The authors declare no conflict of interest.

This article is a PNAS Direct Submission.

[1]To whom correspondence should be addressed. Email: Bernd.Pichler@med.uni-tuebingen.de.

This article contains supporting information online at www.pnas.org/lookup/suppl/doi:10.1073/pnas.1418391112/-/DCSupplemental.

cOVA-TCRtg-TH1 cells in a mouse model of OVA-induced acute airway delayed-type hypersensitivity reaction (DTHR) using chicken, turkey (t), and pheasant (ph) OVA to detect cOVA-specific T-cell homing. This labeling approach was successfully transferred to different mouse TCRs and to the expression marker Thy1.2 to label T cells as well as T-cell–depleted lymphocytes of the spleen.

Results

Intracellular Labeling of cOVA-TCRtg-TH1 Cells Using DOTA-Modified and ^{64}Cu-Radiolabeled cOVA-TCR–Specific mAbs. To avoid the problems associated with mAbs binding to the T-cell surface, we intracellularly labeled cOVA-TCRtg-TH1 cells with radiolabeled TCR-specific [^{64}Cu]DOTA-KJ1-26 mAbs that were incorporated within 24 h via endocytosis of the [^{64}Cu]DOTA-KJ1-26 mAb–cOVA-TCR complex (Fig. 1*A*). This approach enables the highly specific labeling of T cells without impairing their function because the cOVA-TCRs were re-expressed at the cell surface within 24 h. To investigate whether the DOTA modification and ^{64}Cu radiolabeling affected the specific binding capacity of the cOVA-TCR–specific KJ1-26 mAbs and, consequently, the labeling efficiency, we incubated cOVA-TCRtg-TH1 cells in vitro with commercial KJ1-26 mAbs or self-produced DOTA-modified and ^{64}Cu-radiolabeled DOTA-KJ1-26 mAbs before a secondary FITC anti-mouse IgG antibody was added for FACS analysis. The KJ1-26 mAbs and KJ1-26 mAb modifications yielded a cOVA-TCRtg-TH1 cell-labeling efficiency of 97–98% (Fig. S1*A*). However, the mean fluorescence intensities (MFI), which represent the amount of KJ1-26 mAbs bound to the surface of the cOVA-TCRtg-TH1 cells, decreased to 60% after DOTA modification [48.9 ± 0.3 arbitrary units (AU)] and to 46% after ^{64}Cu radiolabeling (36.9 ± 1.4 AU) compared with the unmodified KJ1-26 mAbs, which had the highest MFI (80.9 ± 6.1) (Fig. S1*B*).

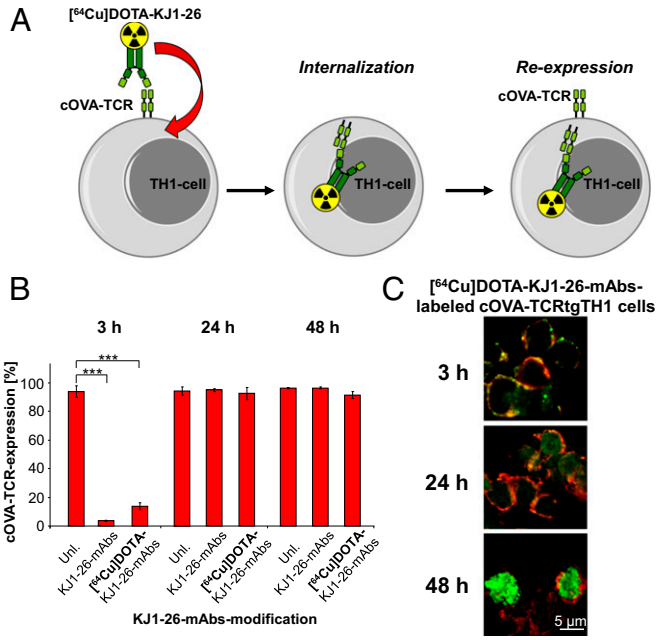

Fig. 1. Internalization dynamic of KJ1-26 mAbs. (*A*) Schematic principle of the in vitro labeling of cOVA-TCRtg-TH1 cells with cOVA-TCR–specific [^{64}Cu]DOTA-KJ1-26 mAbs. (*B*) FACS-quantification of cOVA-TCR expression of unlabeled cOVA-TCRtg-TH1 cells, cOVA-TCRtg-TH1 cells labeled with KJ1-26 mAbs or [^{64}Cu]DOTA-KJ1-26 mAbs after 3, 24, and 48 h (mean ± SD in percent; $n = 4$; Dunnet's test with unlabeled cells as a control; $^{***}P < 0.001$). (*C*) Fluorescence microscopy of [^{64}Cu]DOTA-KJ1-26 mAb-labeled cOVA-TCRtg-TH1 cells. Cryosections of cOVA-TCRtg-TH1 cells were stained 3, 24, and 48 h after the initial labeling procedure for anti-mouse IgG (green, 40×) and CD3 mAbs (red). Merged acquisitions indicate the exact location of [^{64}Cu]DOTA-KJ1-26 mAbs on the cell membrane (yellow) or after internalization in the cOVA-TCRtg-TH1 cells.

Cell-surface cOVA-TCR expression is mandatory for the recognition of the cOVA peptides presented by MHC-II molecules on antigen-presenting cells (APCs) within the lymphatic organs, inflammation sites, or tumor microenvironment. Thus, we investigated the accessibility of the cOVA-specific TCR to KJ1-26 mAbs 3, 24, and 48 h after the initial 30-min labeling period with unmodified KJ1-26 mAbs (0.8 μg) or radiolabeled [^{64}Cu]DOTA-KJ1-26 mAbs (0.7 MBq) to determine the cOVA-TCR turnover at the cell surface. As expected, the accessibility/binding of cOVA-TCR–specific KJ1-26 mAbs to the cell surface OVA-TCR was dramatically reduced to 13.8 ± 1.2% compared with unlabeled control cells (93.7 ± 2.1%) 3 h after labeling with [^{64}Cu]DOTA-KJ1-26 mAbs. Similar results were achieved using unmodified KJ1-26 mAbs (Fig. 1*B* and Fig. S1*C*). Within 24 h after labeling with [^{64}Cu]DOTA-KJ1-26 mAbs, the accessibility/binding to membranous cOVA-TCR recovered completely to 92.3 ± 2.2% and remained stable at 48 h (91.3 ± 1.2%). Unmodified KJ1-26 mAbs yielded similar results (Fig. 1*B* and Fig. S1*C*).

Confocal microscopy directly illustrated the endocytosis of the [^{64}Cu]DOTA-KJ1-26 mAb–cOVA-TCR complex in cOVA-TCRtg-TH1 cells. We labeled the cells with 0.7 MBq of [^{64}Cu]DOTA-KJ1-26 mAbs, 0.8 μg of KJ1-26 mAbs and F(ab′)$_2$ fragments and then examined them for membranous CD3 antigen expression and KJ1-26 mAbs localization (Fig. 1*C* and Fig. S2). The [^{64}Cu]DOTA-KJ1-26 mAbs colocalized with CD3 at the cell membrane 3 h after labeling (Fig. 1*C*, yellow). At 24 h after T-cell labeling, the [^{64}Cu]DOTA-KJ1-26 mAb–cOVA-TCR complex was incorporated and appeared in the cytoplasm (green), whereas only faint [^{64}Cu]DOTA-KJ1-26 mAbs expression was found at the membrane (Fig. 1*C*, yellow). At 48 h, the [^{64}Cu]DOTA-KJ1-26 mAb–cOVA-TCR complex was observed only in the cytoplasm and in a random distribution. Similar results were observed with regard to nonradiolabeled KJ1-26 mAbs (Fig. S2*A*) and, most importantly, KJ1-26-F(ab′)$_2$ fragments, thereby excluding an Fc-receptor–dependent mAb incorporation mechanism (Fig. S2 *B* and *C*).

Establishment of an Optimized Protocol for the Intracellular Labeling of cOVA-TCRtg-TH1 Cells with [^{64}Cu]DOTA-KJ1-26 mAbs. Based on previous studies (10) and the cOVA-TCR–specific intracellular labeling established in the present study, we analyzed the [^{64}Cu]DOTA-KJ1-26 mAb–cOVA-TCR complex-labeling for its use in subsequent in vivo PET studies and its effect on T-cell functioning. Trypan blue exclusion demonstrated that low amounts of activity (0.7 MBq) conferred only a slightly decreased cOVA-TCRtg-TH1 cell viability to 92% at 24 h compared with unlabeled control cells; at 48 h, the viability was reduced to 60% (Fig. 2*A*). Higher amounts of activity (1.5 and 2.1 MBq) impaired the cOVA-TCRtg-TH1 viability more severely at 24 and 48 h. Furthermore, 0.8 μg of nonradiolabeled KJ1-26 mAbs, which was comparable with the level of 0.7 MBq radiolabeled KJ1-26 mAbs, did not impair T-cell viability (Fig. S3*A*).

The cOVA-specific restimulation of [^{64}Cu]DOTA-KJ1-26 mAb-labeled cOVA-TCRtg-TH1 cells, focusing on IFN-γ production at 3, 24, and 48 h after the labeling procedure, showed that the IFN-γ concentrations in the supernatants were normal at 3 and 24 h after labeling (Fig. 2*B*). We observed a significantly impaired IFN-γ production 48 h after application of [^{64}Cu]DOTA-KJ1-26 mAb (Fig. 2*B*). This finding indicates that the [^{64}Cu]DOTA-KJ1-26 mAb-labeling does not affect antigen recognition or T-cell activation up to 24 h after the labeling procedure. Labeling T cells with nonradioactive KJ1-26 mAbs yielded similar results, further excluding the severe effects of the applied amount of radioactivity with regard to specific cOVA-TH1 cell function (Fig. S3*B*).

To determine the effects of [^{64}Cu]DOTA-KJ1-26 mAbs and [^{64}Cu]PTSM-labeling on the mRNA expression patterns of

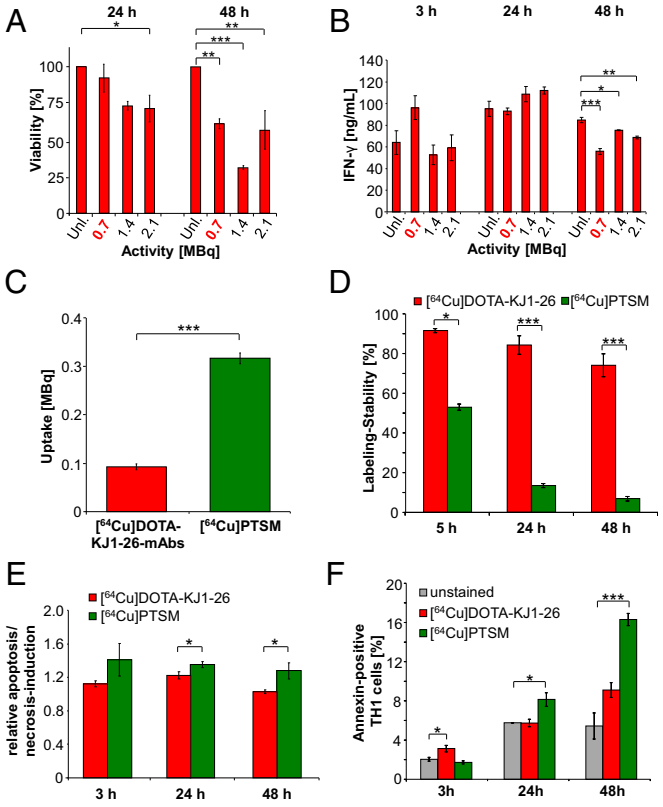

Fig. 2. In vitro evaluation of the [^{64}Cu]DOTA-KJ1-26 mAb–cOVA-TCR complex-labeling. (*A*) Viability 24 and 48 h after applying 0.7, 1.5, or 2.2 MBq of [^{64}Cu]DOTA-KJ1-26 mAbs for 30 min; unlabeled cOVA-TCRtg-TH1 cells served as control (Dunnet's test; $*P < 0.05$; $**P < 0.01$; $***P < 0.001$; mean ± SEM; $n = 3$). (*B*) IFN-γ concentration (ng/mL) in the supernatants of stimulated cOVA-TCRtg-TH1 cells 3, 24, or 48 h after labeling without or with 0.7, 1.5, or 2.2 MBq of [^{64}Cu]DOTA-KJ1-26 mAbs (Dunnet's test; $*P < 0.05$; $**P < 0.01$; $***P < 0.001$; mean ± SEM; $n = 3$). (*C*) Uptake after labeling with 0.7 MBq [^{64}Cu]DOTA-KJ1-26 mAbs ($n = 26$) or 0.7 MBq [^{64}Cu]PTSM ($n = 50$) in 10^7 cOVA-TCRtg-TH1 cells as mean ± SEM in MBq. (*D*) Labeling stability after 5, 24, and 48 h after application of [^{64}Cu]DOTA-KJ1-26 mAbs and [^{64}Cu]PTSM ($n = 3$–5). Data are normalized to the initial activity in cOVA-TCRtg-TH1 cells acquired immediately after the labeling procedure (student's *t* test; $*P < 0.05$; $***P < 0.001$ mean ± SEM in percent). (*E*) FACS-analysis of apoptosis/necrosis induction (TMRE) 3, 24, and 48 h after labeling with 0.7 MBq of [^{64}Cu]DOTA-KJ1-26 mAbs or [^{64}Cu]PTSM compared with an unlabeled control (mean ± SD; $n = 3$; student´s *t* test; $*P < 0.05$). (*F*) FACS analysis for annexin V expression 3, 24, and 48 h after labeling with 0.7 MBq of [^{64}Cu]DOTA-KJ1-26 mAbs or [^{64}Cu]PTSM (Dunnet's test; $*P < 0.05$; $***P < 0.001$; mean ± SEM in percent; $n = 3$).

T cells, we analyzed TH1 cell-associated mediators (IFN-γ, IL-17, IL-2, TNF) and observed an up-regulation of IFN-γ, IL-17, and TNF mRNA expression 3 h after the labeling with [^{64}Cu]DOTA-KJ1-26 mAb (*SI Results* and Fig. S3*C*).

The sufficient and stable uptake of the [^{64}Cu]DOTA-KJ1-26 mAb–cOVA-TCR complex is essential to enable in vivo PET cell-tracking studies. Consequently, we examined the [^{64}Cu]DOTA-KJ1-26 mAbs uptake of 10^7 cOVA-TCRtg-TH1 cells (the amount of T cells injected for in vivo studies) after labeling with 7 MBq [^{64}Cu]DOTA-KJ1-26 mAbs compared with 10^7 cOVA-TCRtg-TH1 cells labeled with 7 MBq [^{64}Cu]PTSM for 3 h of incubation time, as previously described (10). The uptake of [^{64}Cu]DOTA-KJ1-26 mAbs (0.09 ± 0.006 MBq) into the 10^7 cOVA-TCRtg-TH1 cells was three-times lower than that of [^{64}Cu]PTSM (0.32 ± 0.011 MBq) (Fig. 2*C*). However, the [^{64}Cu]DOTA-KJ1-26 mAb–cOVA-TCR complex-labeling of the cOVA-TCRtg-TH1 cells yielded up to a 10-fold higher labeling stability compared with [^{64}Cu]PTSM. Five hours after [^{64}Cu]DOTA-KJ1-26 mAbs-labeling, 91.6 ± 1.0% of the ^{64}Cu remained within the cOVA-TCRtg-TH1 cells, 84.3 ± 4.6% after 24 h, and 74.1 ± 5.7% after 48 h (Fig. 2*D*). The substantial differences in the efflux between [^{64}Cu]DOTA-KJ1-26 mAbs and [^{64}Cu]PTSM were observed at all investigated time points (Fig. S3*D*).

DNA Damage and Apoptosis/Necrosis Induction After Internalization of the [^{64}Cu]DOTA-KJ1-26 mAbs. The application of radioactive cell-labeling compounds, such as [^{64}Cu]PTSM and [^{111}In]oxine, induces DNA damage (10). Many cell-labeling studies have neglected this important aspect, which can result in either apoptosis or necrosis. Radiation-induced DNA double-strand breaks can be characterized via the detection of the phosphorylated histones of the γH2AX-family using flow cytometry. Indeed, intracellular [^{64}Cu]DOTA-KJ1-26 mAb–cOVA-TCR complex-labeling showed a 3.2-fold lower γH2AX-signal in cOVA-TCRtg-TH1 cells (relative H2AX-expression: 2.8 ± 0.3) (Fig. S3*E*) compared with [^{64}Cu]PTSM-labeled cOVA-TCRtg-TH1 (8.9 ± 2.8) [published in Griessinger et al. (10)]. Both investigations were performed on the same experimental day. Next, we investigated whether [^{64}Cu]DOTA-KJ1-26 mAbs-labeling induces apoptosis or necrosis in cOVA-TCRtg-TH1 cells. cOVA-TCRtg-TH1 cells were stained with a probe for mitochondrial membrane potential, tetramethylrhodamine ethyl ester (TMRE), or for annexin V expression, after the initial labeling procedure with 0.7 MBq [^{64}Cu]DOTA-KJ1-26 mAbs (incubation for 30 min) or [^{64}Cu]PTSM (incubation for 3 h). In summary, [^{64}Cu]DOTA-KJ1-26 mAbs-labeled cOVA-TCRtg-TH1 cells displayed constant but much lower apoptosis/necrosis induction than [^{64}Cu]PTSM-labeled cOVA-TCRtg-TH1 cells over the investigation time period (Fig. 2*E*). The labeling with [^{64}Cu]DOTA-KJ1-26 mAbs caused a moderate increase in annexin V expression already after 3 h compared with [^{64}Cu]PTSM-labeled cells or unlabeled controls. However, after 24 h, annexin V expression by [^{64}Cu]DOTA-KJ1-26 mAb-labeled TH1 cells was on the same level as observed for unlabeled controls, whereas [^{64}Cu]PTSM-labeling strongly enhanced annexin V expression (Fig. 2*F*).

Investigation of cOVA-Specific cOVA-TCRtg-TH1 Cell Homing Patterns in OVA-Induced Airway DTHR. The in vitro optimization of the intracellular [^{64}Cu]DOTA-KJ1-26 mAb–cOVA-TCR complex-labeling protocol revealed that the application of 0.7 MBq of [^{64}Cu]DOTA-KJ1-26 mAbs only minimally impaired cOVA-TCRtg-TH1 cell functioning but loads the cells with radioactivity. We next determined whether this protocol enables noninvasive in vivo TH1 cell-trafficking PET studies because the stable ^{64}Cu retention within the TH1 cells should provide an optimal signal-to-background ratio for the in vivo detection of small TH1 cell accumulations using PET. We injected cOVA-TCRtg-TH1 cells immediately after [^{64}Cu]DOTA-KJ1-26 mAbs T-cell–labeling and examined the in vivo homing of cOVA-TCRtg-TH1 cells to the cOVA presentation sites during cOVA-DTHR using PET. Importantly, the cOVA-TCRtg-TH1 cells in this context respond exclusively to OVA derived from chicken (i.e., cOVA) but do not react to OVA derived from turkey (tOVA) or pheasant (phOVA) OVA (11). cOVA stimulated IFN-γ production in cOVA-TCRtg-TH1 cells, but tOVA and phOVA did not (Fig. S4). To test the specificity of the in vivo cOVA-TCRtg-TH1 cell homing to the cOVA presentation via APCs, we induced airway DTHR in littermates with cOVA, tOVA, or phOVA. A histological analysis confirmed that cOVA and tOVA induced a strong inflammatory response, whereas phOVA induced only a weak airway DTHR in the lung and perithymic lymph nodes (LNs) (Figs. S5 and S6). To investigate the specific homing of cOVA-TCRtg-TH1 cells to the cOVA-induced inflammation site using PET, we injected 10^7 [^{64}Cu]DOTA-KJ1-26 mAb-labeled cOVA-TCRtg-TH1 cells intraperitoneally into cOVA-, tOVA-, or phOVA-DTHR–diseased and untreated animals and performed PET/CT scans after 3, 24, and 48 h. No differences were observed

with regard to cOVA-TCRtg-TH1 cell homing in the pulmonary and perithymic LNs across the three OVA-immunized experimental groups after 3 h. However, the signals in the pulmonary and perithymic LNs were higher than those in the untreated control group (Fig. 3), most likely indicating the initial unspecific infiltration of the cOVA-TCRtg-TH1 cells into the inflamed pulmonary and perithymic LNs. Furthermore, the [^{64}Cu]DOTA-KJ1-26 mAbs might still have blocked the recognition of the cOVA-antigen by cOVA-TCRtg-TH1 cells 3 h after labeling. However, cOVA-TCRtg-TH1 cells were only enriched in the peptide-presenting lymphatic structures of the cOVA-immunized mice after 24 and 48 h. In particular, we detected 1.8- and 1.6-fold increases in cOVA-TCRtg-TH1 cell homing within the pulmonary LNs of cOVA-DTHR–diseased mice compared with their untreated littermates at 24 and 48 h, respectively (48 h: cOVA-DTHR 10.6 ± 1.3%ID/cm^3 vs. 6.5 ± 0.9%ID/cm^3, untreated; P = 0.0210) (Fig. 3 *A* and *C*). [^{64}Cu]DOTA-KJ1-26 mAbs-labeled cells could be exclusively identified by immunhistochemistry in peribronchal and subpleural areas of the lung of cOVA-diseased animals (Fig. S7). Similar cOVA-specific cOVA-TCRtg-TH1 cell homing patterns were observed in the perithymic LNs. At 24 h after the administration of cOVA-TCRtg-TH1 cells, cOVA-DTHR-diseased animals showed 1.4-times more homing in the perithymic LNs than in the untreated mice (cOVA-DTHR 12.4 ± 1.2%ID/cm^3; untreated 9.1 ± 1.4%ID/cm^3; P = 0.0448) (Fig. 3 *B* and *D*). Importantly, the signals (%ID/cm^3) in the pulmonary and perithymic LNs of the tOVA- and phOVA-DTHR–diseased animals had similar ranges to those observed in untreated animals 24 and 48 h after cOVA-TCRtg-TH1 cell injection (Fig. 3).

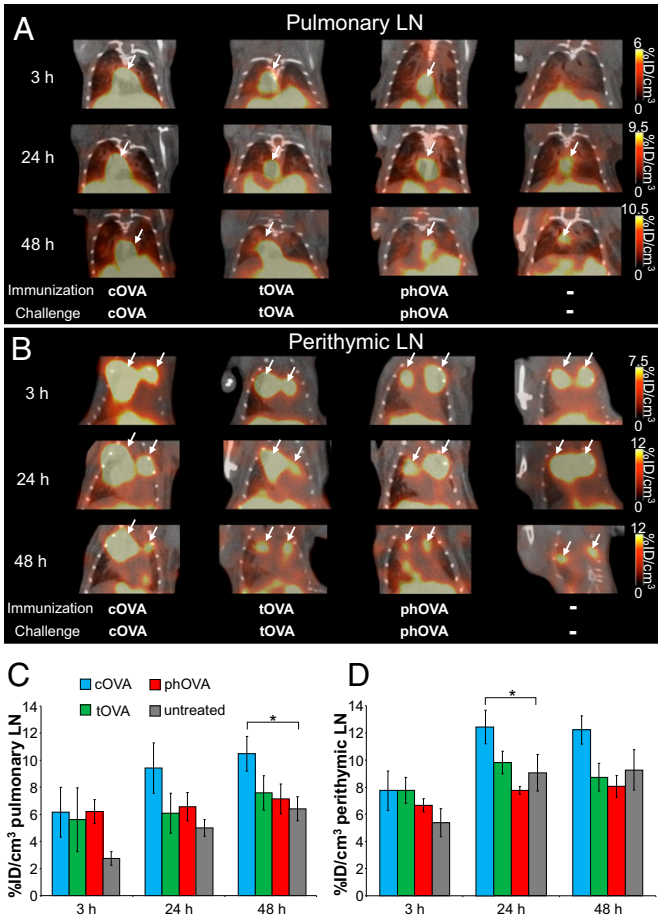

Fig. 3. The detection of the specific homing of [^{64}Cu]DOTA-KJ1-26 mAb–cOVA-TCR complex-labeled cOVA-TCRtg-TH1 cells in cOVA-DTHR–diseased animals. (*A* and *B*) PET/CT scans of the cOVA-TCRtg-TH1 cells in the pulmonary and perithymic LNs (white arrows) 3, 24, and 48 h after intrapteritoneal transfer into cOVA-, tOVA-, or phOVA-DTHR–diseased and untreated animals. (*C* and *D*) Enhanced homing of cOVA-TCRtg-TH1 cells was observed in the pulmonary and perithymic LNs of cOVA-DTHR–diseased animals after 24 and 48 h, whereas no differences were detected between tOVA, phOVA and untreated animals (mean ± SEM in %ID/cm^3; Dunnet's test with "untreated" as control; *P < 0.05; cOVA-DTHR n = 18, tOVA-DTHR n = 6, phOVA-DTHR n = 6, untreated n = 11).

In a second in vivo approach, [^{64}Cu]DOTA-KJ1-26 mAbs-labeled cOVA-TCRtg-TH1 cells were cultured for additional 24 h after the initial labeling procedure to enable the re-expression of the OVA-TCR. In PET/CT studies we were able to track and quantifiy the cOVA-TCRtg-TH1 cell homing for only 24 h (*SI Results* and Fig. S8 *A–D*).

Transfer of the [^{64}Cu]DOTA mAbs-Based Labeling-Method to Large T-Antigen–Specific Th1 Cells and Alternative Immune Cells. To visualize T-cell homing to self-antigens using the mAb-based labeling approach, we used a mouse model for endogenous β-cell carcinomas, in which all β-cells of the pancreas express the large T-antigen (Tag2) under control of the rat insulin promotor 1 (RIP1) (4, 6, 12). In the RIP1-Tag2 animal model, the Tag2-antigen represents the self-antigen, which underlies the tolerance of the host immune system. Thus, fully established β-cell carcinomas show no infiltration of B and T cells (6). We have established a successful Tag2-Th1 cell-based immunotherapy of RIP1-Tag2 mice (4, 6) which doubles the life span of RIP1-Tag2 mice. We used Tag2–T-cell receptor transgenic mice (Tag2-TCRtg) as the source of therapeutic Tag2-TH1 cells (IFN-γ–producing CD4$^+$ T cells) (4) and labeled the Tag2-TCRtg-TH1 cells with a [^{64}Cu]DOTA-modified Tag2-TCR-specific mAb 9H5.1 (13). We confirmed the re-expression of Tag2-TCR (Fig. S8*E*) and internalization of 9H5.1 mAbs within 24 h after labeling (Fig. 4*A*). We were able to visualize the homing of 10^7 intraperitoneally transferred Tag2-TH1 cells into the pancreatic area (Fig. 4*B*) and into the perithymic LNs, the first homing site of intraperitoneally administered T cells (Fig. 4*C*) within 24 h (10).

To label T cells and B cells (T-cell–depleted lymphocytes of the spleen), we used the mAbs specific for mouse Thy1.2 (clone: 53–2.1). We were able to successfully demonstrate the internalization process of the applied mAbs into different immune cell populations within 24 h after labeling (Fig. 4*D*). Thus, radiolabeled mAbs should enable intracellular labeling of immune cells for in vivo PET cell-tracking studies, because internalization dynamics correspond with the observations made for cOVA-TCRtg-TH1 cells.

Discussion

Recently, cell migration visualization has gained increasing interest with regard to cellular immunotherapy and stem cell transplantation. Thus, novel labeling strategies for different imaging modalities should meet several requirements, such as reduced side effects to target cells, high intracellular retention, the possibility of long tracking periods, and easy transfer to clinical practice. We developed a new specific and direct intracellular labeling strategy for mouse T cells by applying TCR-specific mAbs that are internalized in the cells via endocytosis within 24 h. Because of the high regular turnover rate of the TCR and the subsequent expression of free TCR molecules on the cell membrane, TCR internalization enables intracellular labeling of T cells (14, 15). Intracellular labeling via the application of radiolabeled mAbs provides a low efflux of the label and, consequently, a high in vivo signal-to-background contrast among PET studies. Furthermore, the internalization of the mAb–TCR complex avoids host immune reactions that might be induced by mAbs on the outer cell surface. As a consequence of cell-surface labeling, antibody-induced immune reactions could be mediated by the mAb directly, the complement system, or immune cells with Fc-receptors, leading to the destruction of the labeled cells after adoptive transfer (16).

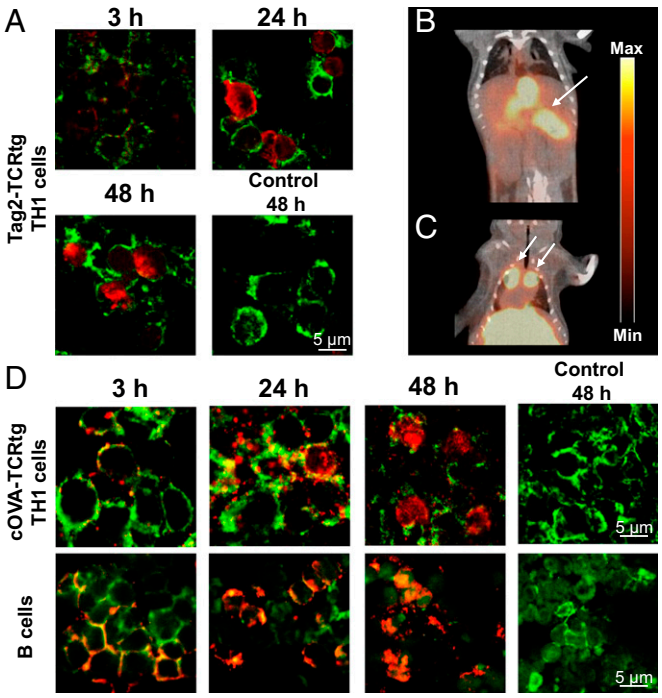

Fig. 4. Application of mAbs-based antibody labeling to other TCRtg-T cells and immune cell types. (*A*) Fluorescence microscopy of 9H5.1-labeled Tag2-TCRtg-TH1 cells. Cryosections of Tag2-TCRtg-TH1 cells were stained 3, 24, and 48 h after the initial labeling procedure for anti-mouse IgG (red, 40×) and CD3 (green). (*B* and *C*) In vivo PET/CT 24 h after injection of 10^7 [^{64}Cu]DOTA-9H5.1 mAbs-labeled Tag2-TCRtg-TH1 cells in a RIP1-Tag2 mouse. Tag2-TCRtg-TH1 cells home to the pancreatic area and to administration-specific homing sites (perithymic LN). (*D*) Fluorescence microscopy of the internalization of 53–2.1 mAbs in Thy1.2$^+$ cOVA-TCRtg-TH1 cells (*Upper*) and T-cell–depleted lymphocytes of the spleen (*Lower*, mainly B cells). Cryosections of Tag2-TCRtg-TH1 and B cells were stained 3, 24, and 48 h after the initial labeling procedure for anti-rat IgG (red, 40×) and CD3 (T cells, green) or phalloidin (B cells, green).

In our labeling approach we applied 0.7 MBq (0.8 μg) of cOVA-TCR–specific [^{64}Cu]DOTA-KJ1-26 mAbs per 10^6 cOVA-TCRtg-TH1 cells for only 30 min, ensuring a sufficient uptake of ^{64}Cu (Fig. 2*C*) and labeling stability via the internalization of the [^{64}Cu]DOTA-KJ1-26 mAbs within 24 h. In contrast, other radiotracers used for cell labeling, such as [^{64}Cu]PTSM, [^{111}In]oxine, or [^{18}F]FDG, show a significantly lower intracellular trapping stability (7, 10, 17). This high trapping stability enables the use of less activity combined with a short exposure time, thereby preventing cell damage while still yielding quantitative, high-quality, low-noise PET images.

Although the application of [^{64}Cu]DOTA-KJ1-26 mAbs limits the accessibility of the cOVA-TCR for antibody binding after 3 h, antigen recognition was possible, as shown by the cOVA-specific IFN-γ production of cOVA-TCRtg-TH1 cells after activation with cOVA and APC. In contrast to [^{64}Cu]PTSM-labeling, the cOVA-specific IFN-γ production was not inhibited within the first 24 h after labeling with different amounts of activity. Rather, we assume that the binding of [^{64}Cu]DOTA-KJ1-26 mAbs to the cOVA-TCRtg-TH1 cells induces cell activation via TCR signaling. This assumption is supported by the enhanced IFN-γ, IL-17, and TNF mRNA-expression 3 h after labeling with [^{64}Cu]DOTA-KJ1-26 mAbs. Our in vitro data on viability, functionality and apoptosis do not support the potential of activation-induced cell death within 48 h. A possible advantage of the activation induced cell death is a reduced risk for overwhelming autoinflammatory reactions (18). In addition, because of the activation-induced cell death, the labeled T cells could lose their therapeutic efficiency over time which can be avoided by coinjection of unlabeled cells along with the labeled cells.

Yudushkin and Vale demonstrated that internalized TCRs are associated with the endosomal compartment in the cytoplasm (19). The slow accumulation dynamics of the mAbs into the cell might explain the less-severe damage to the cOVA-TCRtg-TH1 cells compared with [^{64}Cu]PTSM-labeling, in which ^{64}Cu accumulates rapidly in the cell nucleus (10). The delayed accumulation of the radioactive ^{64}Cu in the T cells might also explain the reduced induction of DNA damage, annexin expression, and apoptosis/necrosis compared with [^{64}Cu]PTSM-labeling. Because of the radiolysis of the mAbs (20), free ^{64}Cu might also have accumulated in the cell nucleus but to a much lesser extent than [^{64}Cu]PTSM. Furthermore, the radioactivity and the Cu itself might be capable of inducing DNA damage and apoptosis (21–23).

The uptake in 10^7 OVA-TH1 cells after the application of 7 MBq of [^{64}Cu]DOTA-KJ1-26 mAbs for labeling was sufficient but relatively low. However, the high sensitivity of PET enabled the in vivo detection and quantification of the homing sites of adoptively transferred cOVA-TCRtg-TH1 cells. In addition to the manifold advantages of the in vitro labeling strategy compared with [^{64}Cu]PTSM, we observed additional improvements with regard to the in vivo migration studies. Because of the high labeling stability, yielding a low background signal in imaging studies, of the [^{64}Cu]DOTA-KJ1-26 mAb–cOVA-TCR complex-labeling, we were able to demonstrate an increased cOVA-specific homing of cOVA-TCRtg-TH1 cells to the inflamed pulmonary and perithymic LNs of mice diseased with cOVA-DTHR, but not those with phOVA- or tOVA-induced airway DTHR, 24 h and 48 h after injection.

The cOVA-TCRtg-TH1 cell homing in animals with a strong airway DTHR after treatment with tOVA and a low airway DTHR after treatment with phOVA was similar to that in untreated animals after 24 and 48 h. We did not observe specific homing patterns 3 h after the injection of cOVA-TCRtg-TH1 cells, most likely because of the limited accessibility to the cOVA-TCR because of the binding of the [^{64}Cu]DOTA-KJ1-26 mAbs. The addition of a 24-h culture period after labeling to facilitate the re-expression of the cOVA-TCR might increase the sensitivity but limit the tracking period to 24 h.

Most importantly, we were able to successfully transfer our labeling mAb approach to another T-cell model, in which we labeled Tag2-TCRtg-TH1 cells with [^{64}Cu]DOTA-9H5.1 mAbs. In RIP1-Tag2 mice we could follow the homing of the Tag2-TCRtg-TH1 cells to the pancreatic area. This result confirms previous findings of Müller-Hermelink et al. (4). These authors could successfully detect DiD-fluorescence labeled Tag2-TCRtg-TH1 cells at the Tag2-expressing β-cell carcinomas by optical imaging (4). Furthermore, we showed the internalization of the mAb 53–2.1, specific for anti-mouse Thy1.2, into cOVA-TCRtg-TH1 cells, as well as T-cell–depleted lymphocytes of the spleen. These results indicate that the mAb-based labeling of immune cells is easily transferable to target different membrane markers with a high turnover rate.

Our new labeling approach for PET imaging provides shorter labeling (30 min) and measurement times (20 min) with a high sensitivity to track cells after systemic transfer compared with MRI/NMR cytometry approaches. A detailed comparison of our new mAb-based labeling approach with established MRI/NMR and reporter gene approaches with a focus on advantages and drawbacks of each labeling method is given *SI Discussion*. Briefly, the use of mAbs was successfully established as in vitro cell-labeling approach for cell tracking using MRI (24, 25). Ahrens et al. labeled dendritic cells intracellular with super paramagnetic iron oxide nanoparticle-coupled CD11c-mAb and were able to monitor dendritic cells in vivo for 24 h after intramuscular injection (24). However, the transferred cells could be only detected at the injection site and not systemically. Bulte et al. labeled a transferrin-specific mAb with an MR-contrast agent and detected oligodendrocyte progenitor cells in the spinal cord of myelin deficient rats ex vivo by MRI (25).

An optimization of our cell-labeling approach might involve mAb fragments (26, 27), which carry fewer radionuclides, and thus induce less damage to their target cells. Furthermore, the missing Fc-part of the mAbs would likely prevent the Fc-receptor–mediated cellular cytotoxicity in vivo, thereby increasing the safety of a possible clinical translation. The successful use of mAb fragments to detect immune cells in vivo was shown in the study by Tavaré et al. (27). The authors generated ^{64}Cu-labeled anti-CD8 antibody fragments to detect CD8$^+$ T cells in lymphatic structures in immune competent mice. The missing Fc-part did not lead to depletion of the CD8$^+$ cells in vivo because of prevention of an Fc-receptor mediated immune response (27).

Our T-cell–labeling approach can be easily transferred to a clinical setting. The use of mAbs specific for the α/β-chains of the human TCR or CD45 could provide enormous flexibility to label T cells as well as immune cells of hematopoietic origin. However, specifically targeting a subpopulation of cells is not possible using CD45 mAbs. Thus, we decided to pursue the TCR-specific approach to specifically label T cells.

In conclusion, the present study is, to our knowledge, the first to show that the direct intracellular labeling of T cells with radiolabeled mAbs directed against the TCR enables noninvasive PET cell-tracking studies. Furthermore, we demonstrated the essential advantages of this approach compared with common cell-labeling techniques using [^{64}Cu]PTSM or MRI labels via the induction of less damage to the cells. This approach provides a higher detection sensitivity in vivo, even for systemic cell-tracking studies because of the higher retention of the label that results in low, unspecific background signals and enables the use of less activity for quantitative imaging studies. Comprehensive imaging studies using mouse models of airway DTHR have demonstrated the feasibility of monitoring and quantifying disease-specific temporal cell trafficking via in vivo PET. This labeling strategy offers enormous possibilities and can be easily transferred to other target cells, such as stem and immune cells using radionuclide-modified mAbs directed against cell surface-specific markers with a high cell membrane turnover rate.

Materials and Methods

Detailed methods and experimental procedures including antibody isolation and radiolabeling, T-cell culture and labeling, PET/CT measurements, flow cytometry, and histology are described in detail in the *Supporting Information*. All experiments were performed according to the animal use and care protocols of the German Animal Protection Law and approved by the Regierungspräsidium Tübingen.

TH1 Cell-Labeling Procedure Using [^{64}Cu]DOTA-KJ1-26 mAbs. For the TH1 cell-labeling procedure, 10^6 cOVA-TCRtg-TH1 cells were dispersed on 48-well plates in 0.5 mL of medium. Subsequently, we added 0.7 MBq (approx. 0.8 μg) of [^{64}Cu]DOTA-KJ1-26 mAbs in 20 μL per well for 30 min. For additional in vitro evaluation, we incubated cOVA-TCRtg-TH1 cells with 1.5 (1.6 μg) and 2.2 MBq (2.4 μg) of [^{64}Cu]DOTA-KJ1-26 mAbs. As a control, we incubated cOVA-TCRtg-TH1 cells with respective concentrations of KJ1-26 mAbs (0.8, 1.6 and 2.4 μg) for 30 min. The cells were washed twice, resuspended in PBS, and the cell numbers (10^7 OVA-TCRtg-Th1 cells) were adjusted for intraperitoneal transfer into the diseased animals or prepared for in vitro investigation. In total, 10^7 cOVA-TCRtg-TH1 cells were labeled in 7 MBq of [^{64}Cu]DOTA-KJ1-26 mAbs. In a separate approach, cOVA-TCRtg-TH1 cells were cultured for an additional 24 h to enable the expression of free cOVA-TCR on the cell membrane. They were then adoptively transferred into the experimental animals. For some comparative studies, cOVA-TCRtg-TH1 cells were labeled with 0.7 MBq [^{64}Cu]PTSM for 3 h, as described previously (10).

In Vivo Imaging Using PET/CT. Experimental mice were anesthetized with 1.5% isoflurane (Vetland) in 100% oxygen (flow: 0.7 L/min) in a temperature-controlled anesthesia box. Then, 10^7 [^{64}Cu]DOTA-KJ1-26 mAb–cOVA-TCR complex-labeled cOVA-TCRtg-TH1 cells in 200 μL of PBS were transferred intraperitoneally into cOVA, tOVA, or phOVA-DTHR–diseased and untreated animals. Twenty-minute static PET scans were acquired using a small-animal Inveon microPET scanner (Siemens Medical Solutions). PET scans were performed 3, 24, and 48 h after the intraperitoneal transfer of [^{64}Cu]DOTA-KJ1-26 mAb–cOVA-TCR complex-labeled cOVA-TCRtg-TH1 cells. We also transferred 10^7 cOVA-TCRtg-TH1 cells that were incubated for another 24 h after the initial labeling procedure into cOVA-DTHR–diseased and untreated mice and performed PET/CT scans 3 and 24 h after adoptive cell transfer.

ACKNOWLEDGMENTS. We thank Prof. Edgar Schmitt for providing the KJ1-26 hybridoma cell line; Dr. Karen Alt and Prof. Ursula Elsässer-Beile for their support during the establishment of the DOTA-labeling of monoclonal antibodies in the Werner Siemens Imaging Center; Helmut Schneider for providing turkey eggs; and Birgit Fehrenbacher, Theresia Schneider, Hannelore Bischof, as well as Prof. Martin Eichner and Carsten Calaminus, for the support during the experiments and data analysis. The SFB685 (B6 and C1), the Swiss Werner Siemens-Foundation, and the Sander Stiftung (2005.043.2 and 2005.043.3) funded these experiments.

1. Ahrens ET, Bulte JW (2013) Tracking immune cells in vivo using magnetic resonance imaging. *Nat Rev Immunol* 13(10):755–763.
2. Restifo NP, Dudley ME, Rosenberg SA (2012) Adoptive immunotherapy for cancer: Harnessing the T cell response. *Nat Rev Immunol* 12(4):269–281.
3. Lafaille JJ (1998) The role of helper T cell subsets in autoimmune diseases. *Cytokine Growth Factor Rev* 9(2):139–151.
4. Müller-Hermelink N, et al. (2008) TNFR1 signaling and IFN-gamma signaling determine whether T cells induce tumor dormancy or promote multistage carcinogenesis. *Cancer Cell* 13(6):507–518.
5. Muranski P, Restifo NP (2009) Adoptive immunotherapy of cancer using CD4(+) T cells. *Curr Opin Immunol* 21(2):200–208.
6. Braumüller H, et al. (2013) T-helper-1-cell cytokines drive cancer into senescence. *Nature* 494(7437):361–365.
7. Adonai N, et al. (2002) Ex vivo cell labeling with 64Cu-pyruvaldehyde-bis(N4-methylthiosemicarbazone) for imaging cell trafficking in mice with positron-emission tomography. *Proc Natl Acad Sci USA* 99(5):3030–3035.
8. Prince HM, et al. (2008) In vivo tracking of dendritic cells in patients with multiple myeloma. *J Immunother* 31(2):166–179.
9. Huang J, Lee CC, Sutcliffe JL, Cherry SR, Tarantal AF (2008) Radiolabeling rhesus monkey CD34+ hematopoietic and mesenchymal stem cells with 64Cu-pyruvaldehyde-bis(N4-methylthiosemicarbazone) for microPET imaging. *Mol Imaging* 7(1):1–11.
10. Griessinger CM, et al. (2014) In vivo tracking of Th1 cells by PET reveals quantitative and temporal distribution and specific homing in lymphatic tissue. *J Nucl Med* 55(2):301–307.
11. Shimonkevitz R, Kappler J, Marrack P, Grey H (1983) Antigen recognition by H-2-restricted T cells. I. Cell-free antigen processing. *J Exp Med* 158(2):303–316.
12. Hanahan D (1985) Heritable formation of pancreatic beta-cell tumours in transgenic mice expressing recombinant insulin/simian virus 40 oncogenes. *Nature* 315(6015):115–122.
13. Förster I, Hirose R, Arbeit JM, Clausen BE, Hanahan D (1995) Limited capacity for tolerization of CD4+ T cells specific for a pancreatic beta cell neo-antigen. *Immunity* 2(6):573–585.
14. Balagopalan L, Barr VA, Samelson LE (2009) Endocytic events in TCR signaling: Focus on adapters in microclusters. *Immunol Rev* 232(1):84–98.
15. Geisler C (2004) TCR trafficking in resting and stimulated T cells. *Crit Rev Immunol* 24(1):67–86.
16. Schwab I, Nimmerjahn F (2013) Intravenous immunoglobulin therapy: How does IgG modulate the immune system? *Nat Rev Immunol* 13(3):176–189.
17. Botti C, et al. (1997) Comparison of three different methods for radiolabelling human activated T lymphocytes. *Eur J Nucl Med* 24(5):497–504.
18. Suntharalingam G, et al. (2006) Cytokine storm in a phase 1 trial of the anti-CD28 monoclonal antibody TGN1412. *N Engl J Med* 355(10):1018–1028.
19. Yudushkin IA, Vale RD (2010) Imaging T-cell receptor activation reveals accumulation of tyrosine-phosphorylated CD3ζ in the endosomal compartment. *Proc Natl Acad Sci USA* 107(51):22128–22133.
20. Chakrabarti MC, Le N, Paik CH, De Graff WG, Carrasquillo JA (1996) Prevention of radiolysis of monoclonal antibody during labeling. *J Nucl Med* 37(8):1384–1388.
21. Ostrakhovitch EA, Cherian MG (2005) Inhibition of extracellular signal regulated kinase (ERK) leads to apoptosis inducing factor (AIF) mediated apoptosis in epithelial breast cancer cells: The lack of effect of ERK in p53 mediated copper induced apoptosis. *J Cell Biochem* 95(6):1120–1134.
22. Haldsrud R, Krøkje A (2009) Induction of DNA double-strand breaks in the H4IIE cell line exposed to environmentally relevant concentrations of copper, cadmium, and zinc, singly and in combinations. *J Toxicol Environ Health A* 72(3-4):155–163.
23. Roos WP, Kaina B (2013) DNA damage-induced cell death: From specific DNA lesions to the DNA damage response and apoptosis. *Cancer Lett* 332(2):237–248.
24. Ahrens ET, Feili-Hariri M, Xu H, Genove G, Morel PA (2003) Receptor-mediated endocytosis of iron-oxide particles provides efficient labeling of dendritic cells for in vivo MR imaging. *Magn Reson Med* 49(6):1006–1013.
25. Bulte JW, et al. (1999) Neurotransplantation of magnetically labeled oligodendrocyte progenitors: Magnetic resonance tracking of cell migration and myelination. *Proc Natl Acad Sci USA* 96(26):15256–15261.
26. Wolf P, et al. (2010) Three conformational antibodies specific for different PSMA epitopes are promising diagnostic and therapeutic tools for prostate cancer. *Prostate* 70(5):562–569.
27. Tavaré R, et al. (2014) Engineered antibody fragments for immuno-PET imaging of endogenous CD8+ T cells in vivo. *Proc Natl Acad Sci USA* 111(3):1108–1113.